Journal Homepage: - www.journalijar.com
INTERNATIONAL JOURNAL OF ADVANCED RESEARCH (IJAR)
Article DOI: 10.21474/IJAR01/9960
DOI URL: http://dx.doi.org/10.21474/IJAR01/9960

RESEARCH ARTICLE

COMPARATIVE STRUCTURAL STUDIES OF $LINI_{0.8}CO_{0.1}MN_{0.1}O_2$ CATHODE MATERIALS PREPARED BY SOL-GEL VERSUS SOLID-STATE-REACTION METHOD.

V. Kondala Rao[1], N. Murali[2], V. Veeraiah[1] and K. Samatha[1].

1. Department of Physics, Andhra University, Visakhapatnam.
2. Department of Engineering Physics, Andhra University College of Engineering (A), Andhra University, Visakhapatnam.

Manuscript Info

Manuscript History
Received: 18 August 2019
Final Accepted: 20 September 2019
Published: October 2019

Key words:-
Ni-rich; Cathode material, XRD, FTIR, UV.

Abstract

In the present work, the layered structure oxide $LiNi_{0.8}Co_{0.1}Mn_{0.1}O_2$ (NCM 811) is synthesized by sol-gel auto combustion and solid state reaction methods. Microstructural and optical properties are investigated by XRD, FE-SEM with EDS, FT-IR and bonding nature studies. Characterization of the crystalline powders, phase identification, particle size examination, and morphological studies are done using XRD and FE-SEM. From FT-IR and UV-NIR studies, vibrational bands are identified in the range of 400-2000 cm-1 representing the MO_2 (M = Ni, Co & Mn) layers.

Introduction:-

Lithium-ion batteries (LIBs) have been predominately applied in electric vehicles (EVs) and hybrid electric vehicles (HEVs) due to their high energy density, long cycle life, and energy safety and good rate capability [1-5]. Some researchers have been found Ni-rich cathode materials are the power of Lithium-ion batteries superior energy density due to its high capacity and low cost [6-8]. But, these materials are so many problems are there, such as poor cycling, commercially poor thermal stability, cation mixing [9-10]. Such as these problems are rectify in cations (substitute Ni ions by Ti, Cr, Na, Zr, Mg and non-metallic ion, like F) [11-13] bulk doping (obviously increase the lithium layer spacing, resulting in rapid lithium-ion diffusion into the electrode) [14-15] and surface coating (achieve superior performances due to less unwanted surface functional groups, hydrogen fluoride (HF) scavenger and physical obstacle and conducting media for lithium-ion and electron) [16-18] have been solved these issues. Therefore, great efforts have been reported that it can cause long cycle life owing to enhanced thermal and structural stability and reduced transition metal dissolution [19-20].

Finally, in this paper, we prepared $LiNi_{0.8}Co_{0.1}Mn_{0.1}O_2$ (NCM-811) cathode materials prepared by two different methods such as sol-gel auto-combustion and solid-state reaction methods. Therefore, we believe that the NCM-811 cathode material is a beneficial approach for high performance and reliability of lithium-ion batteries.

Preparation and Characterizations

Sol-gel auto-combustion method: We synthesized $LiNi_{0.8}Co_{0.1}Mn_{0.1}O_2$ cathode materials by using the sol-gel method. A stoichiometric amount of $LiNO_3$ (AR) and $Ni(NO_3)_2.6H_2O$ (AR), $Co(NO_3)_2.6H_2O$ (AR) and $MnC_6H_4.4H_2O$ (AR) are dissolved in distilled water. The aqueous solution of citric acid which is acting as chelating agent is added to the mixer of the metal ion solution according to their molar ratio of 1:1. At the same time, an Ammonia solution as a precipitation agent is separately added. The reaction temperature is kept at 80°C and pH is

Corresponding Author:-V. Kondala Rao.
Address:-Department of Physics, Andhra University, Visakhapatnam.

controlled by ammonia solution to 8 ~ 9. The solutions are added together under stirring at 130°C for 10 hours, forming a sol solution. The sol solution is vaporized at 130°C till the dry gel is formed, followed by the heat treatment at 500° C for 6h in the air with a 5°C/ min heating rate to eliminate the organic residues. The powders are thoroughly ground and then sintered at 850 °C for 20 hours in the air to obtain the required compounds.

Solid-state reaction method: The cathode compositions are synthesized by a solid-state reaction method from stoichiometric amounts of Li_2CO_3 (Merck 99.9%) and NiO (Merck 99.9%), CoO (Merck 99.9%) and MnO(Merck 99.9%). A slight excess amount of lithium (5%) was used to compensate for any loss of the metal which might have occurred during the calcination at high temperatures. The mixture of the starting materials is sufficiently mixed and after grinding the powder it is then heat-treated in the air at 500 ºC for 5 h and it is again ground and mixed, and calcined again at 750 ºC for 20 h. Then, this powder was cooled at a rate of 5 ºC/ min. Finally, the powder was ground and mixed, and calcined again at 850 ºC for 20 h in the air using a muffle box furnace.

The powder X-ray diffraction (XRD) data of the samples are collected on a Rigaku Cu-Kα diffractometer with diffraction angles of 20º and 80º in increments of 0.02º. The unit cell lattice parameter is obtained by the least square fitting method from the d-spacing and (hkl) values. Further, the crystal size of the sample is obtained by applying the Scherrer's equation from the XRD pattern. The particle morphology of the powders is observed using a field effect scanning electron microscopy images taken from CarlZeiss, EVOMA 15, Oxford Instruments, Inca Penta FETx3.JPG. Fourier transform infrared (FT-IR) spectra are obtained on a Shimadzu FT-IR-8900 spectrometer using KBr pellet technique in the wavenumber range between 350 and 800 cm^{-1}.

Results and Discussions:-

TG studies

Figure 1 represents the TG curves of $LiNi_{0.8}Co_{0.1}Mn_{0.1}O_2$ gel precursors synthesized by sol-gel auto combustion method using citric acid as a chelating agent. The formation of synthesized material takes place around 500^0C, which is observed from the TG curve. The major weight loss (around 50%) occurs from 290–485◦C, which leads to the decomposition of acetates corresponding exothermic peak appears around 485◦C. After 485◦C TG curves become flat which indicates that no weight loss occurs in this region; further heating only assists the crystallization event of the $LiNi_{0.8}Co_{0.1}Mn_{0.1}O_2$ material. Similarly, solid state reaction method the first weight loss region from 0 to 100◦C corresponds to the loss of absorbed water molecules. The next weight loss region (100–290◦C) indicates that the decomposition of the chelating agent. From figure 2 shown from the curves, there is an initial weight loss in the temperature range from room temperature to 310°C. This corresponds to the evaporation of methanol used during grinding to homogenize the mixture and the moisture absorbed during storage [21]. TG curve of the synthesized materials are shows significant weight loss (17.8%) between the temperatures 310°C and 570°C. This loss may be due to the decomposition of the precursors Li_2CO_3, NiO_2, Co_2O_3 and MnO_2, and the reaction between the decomposed materials thereby to produce crystalline materials. Though, Li_2CO_3 is stable in air up to 750°C and the melting point is 723°C, some studies have point out that Li_2CO_3 already reacts below 300°C [22]. At the proposed temperature, the TG curve becomes more flattened, indicating stable phase is formed.

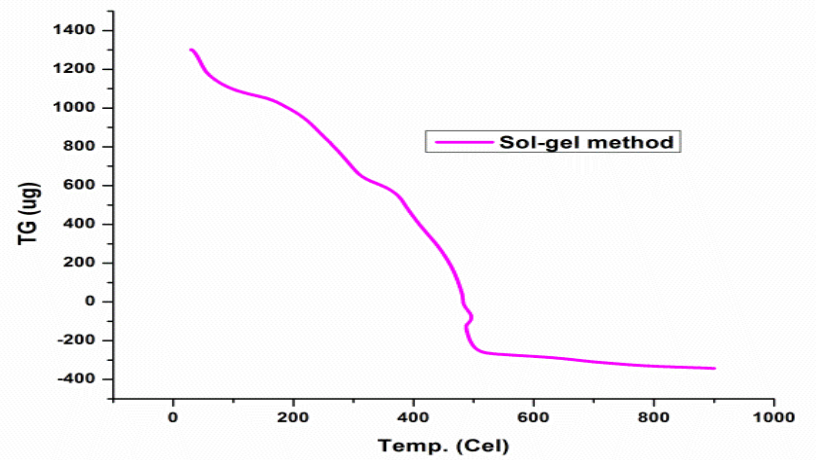

Figure 1:-TG/DTG curve for $LiNi_{0.8}Co_{0.1}Mn_{0.1}O_2$ material is prepared by sol-gel auto-combustion method

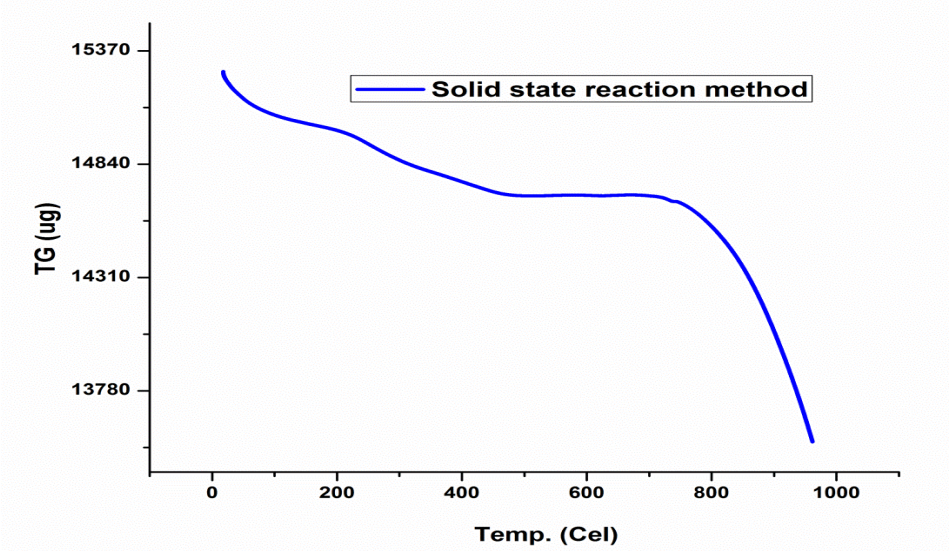

Figure 2:-TG/DTG curve for $LiNi_{0.8}Co_{0.1}Mn_{0.1}O_2$ material is prepared by solid state reaction method

XRD studies

X-ray diffraction patterns for $LiNi_{0.8}Co_{0.1}Mn_{0.1}O_2$ sample is prepared by sol-gel and solid-state reaction methods are shown in Figure 3. Both XRD patterns of the powders prepared by sol-gel auto-combustion and solid-state method show X-ray peaks corresponding to $LiNi_{0.8}Co_{0.1}Mn_{0.1}O_2$ can be indexed to a phase-pure hexagonal structure with the space group of R3m and match well with diffraction file (JCPDS) 74-0919 [23]. The synthesized material is with no evidence of any impurities, indicating that the uniform solid solution has been formed in the compounds [24]. The crystal lattice parameters of the compounds are calculated by using the unit cell program and presented in Table 1. LiO_6, MO_6 where M=Ni, Co and Mn occupy 3b, 3a positions and O is in the 6c position in Fig. 1. Which should be related to the larger radii of Li^+ (0.72Å) is thus their cell volume should be expanded according to Vegard's law. We believe that this would be attributed to the decrease in the Ni^{2+} (0.69Å), Co and Mn (ionic radii) content caused by the charge compensation for the compound in both methods to remain in electrically neutral. The overall high-intensity ratio of the (0 0 3) and (1 0 4) peaks and the clear splitting of the (0 1 8) and (1 1 0) peaks indicate that the compounds have a good structure [25]

The a-axis increases linearly from 2.893 to 2.896 Å and the c-axis decreases from 14.238 to 14.23 Å. The ratio of c/a decreases from 4.922 to 4.915Å due to the substitution of Ni ions by Co and Mn ions probably result from the severe cation mixing because it has the lowest intensity ratio of (0 0 3) to (1 0 4) peaks as given in Table 1. The unit-cell volume also increases from 103.205 to 103.371 $Å^3$. The crystallite sizes of the cathode powders are prepared from the sol-gel auto-combustion and solid-state reaction methods are shown in 9.8 nm and 12.67 nm. The Bragg intensity ratio of I(0 03)/I(1 04), which is a signature of the cation-mixing and Its values are 1.1602 and 1.1361. It has been reported that if this value is < 1.2 for the undesirable cation mixing would occur in the lattice. The crystallite size can be estimated using Scherrer's formula given in eq. (1).

$$D = 0.9/\beta\cos\theta \quad \text{---------- (1)}$$

where, λ is the wavelength of X-ray used, which is CuKα radiation (λ= 1.5406 Å), and β is the full width at half-maximum of the diffraction peak corresponding to 2θ. Using the above equation the sizes of the crystallites are found to be in the range of nanometer [26]. The crystallite size is measured by taking the average of three mainline widths, which are obtained from the XRD patterns. The crystallite size calculated using the Debye Scherrer's formula is listed in the table. 1.

Table 1:-The sol-gel and solid state reaction methods

Samples	a(Å)	c(Å)	c/a	Cell volume $(Å)^3$	I_{003}/I_{104}	R-factor $((I_{006}+I_{102})/I_{101})$	Crystallite size (nm)
NCM811 (SG)	2.875	14.336	4.921	103.31	1.67	20.6	7.43
NCM811 (SSR)	2.893	14.243	4.923	103.26	0.99	20.8	10.77

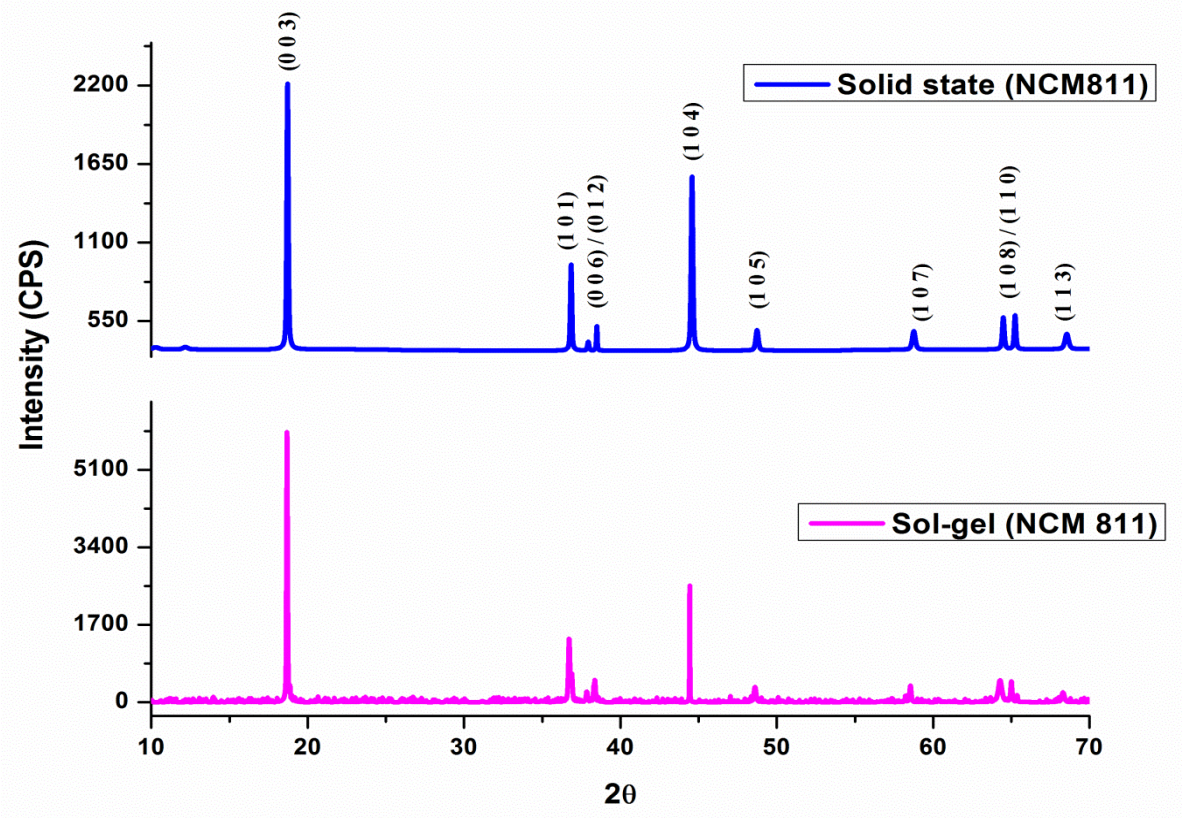

Figure 3:-X-ray diffraction patterns for $LiNi_{0.8}Co_{0.1}Mn_{0.1}O_2$ material is prepared by sol-gel auto-combustion and solid state reaction methods

FE-SEM with EDS studies

Figure 4 and 5 shows the FE-SEM images of the $LiNi_{0.8}Co_{0.1}Mn_{0.1}O_2$ compound in sol-gel auto-combustion and solid-state reaction method. Both compounds have a smooth, well-shaped and particle-agglomerated morphology [27]. The average size of the primary particle is about 500 nm and 2 µm. These samples have the accumulation morphology, but the primary particles become well-shaped and their size increases. In this results suggest that foreign metal ion doping could improve the crystallinity of the synthesized samples. The precursor powders with spherical shape and dense morphologies were necessary to prepare the cathode powders with spherical shape and dense structure by both methods with a lithium component. Figure 3 and 4 shows the EDS spectra, qualitative results and elemental analysis that confirms the presence of Ni, Co, Mn and O in $LiNi_{0.8}Co_{0.1}Mn_{0.1}O_2$ cathode material. It is clearly observed that the spectra show the appropriate ratios of the elements. Lithium is not observed in the EDS spectrum because it has too low of an atomic number to be detected with EDS.

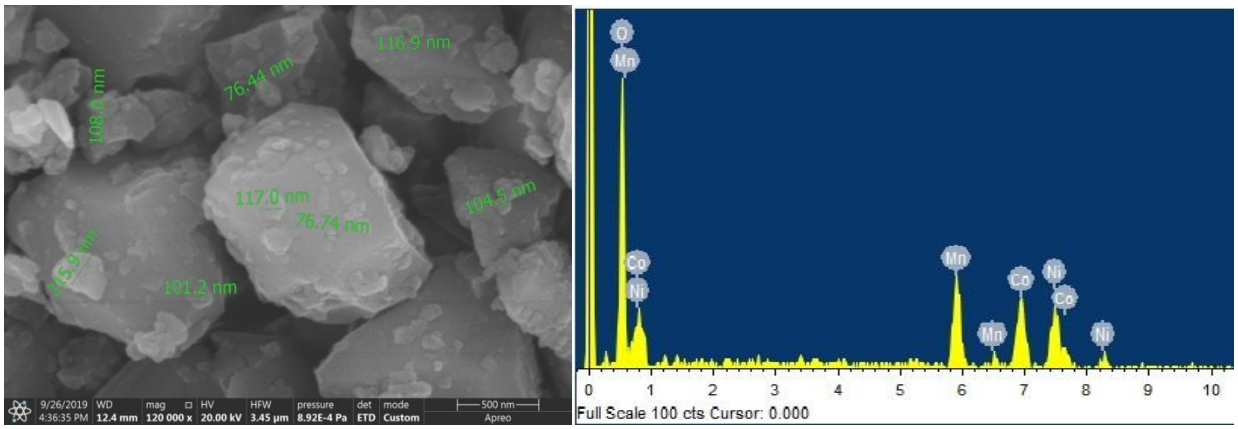

Figure 4:-FE-SEM with image for $LiNi_{0.8}Co_{0.1}Mn_{0.1}O_2$ material is prepared by sol-gel auto-combustion method

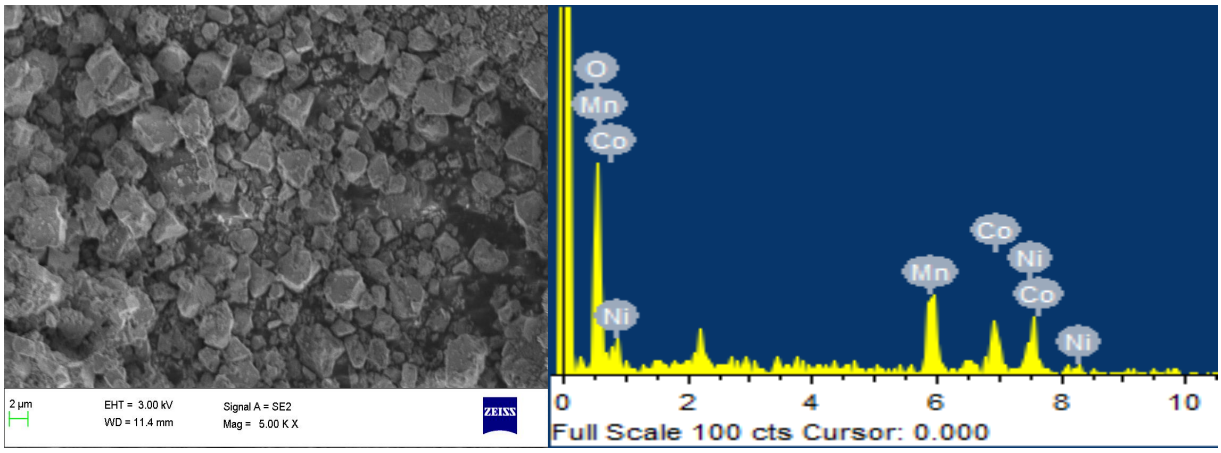

Figure 5:-FE-SEM with image for $LiNi_{0.8}Co_{0.1}Mn_{0.1}O_2$ material is prepared by solid state reaction method

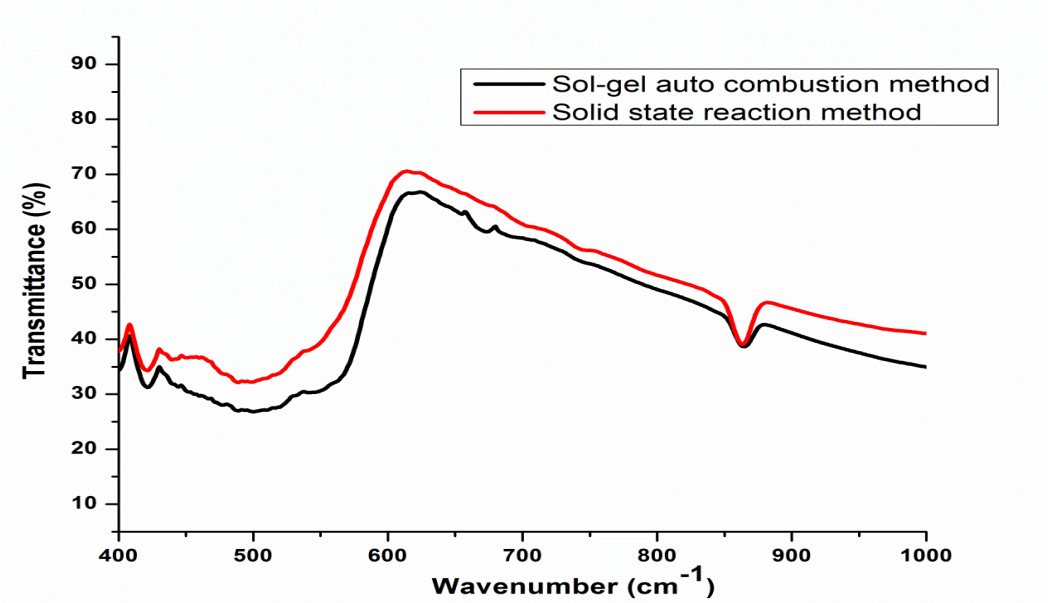

Figure 6:-FT-IR spectra $LiNi_{0.8}Co_{0.1}Mn_{0.1}O_2$ material is prepared by sol-gel auto-combustion and solid state reaction methods

FT-IR studies

From the figure 6 represents the mode of vibrations for transition metals $LiNi_{0.8}Co_{0.1}Mn_{0.1}O_2$ in the 400–1000 cm^{-1} region which is largely associated with the vibrations of MO_6 where M=Ni, Co and Mn and LiO_6 octahedral units. The peaks at 613 cm^{-1} and 614 cm^{-1} are listed in the table. 2 the vibration bending modes of MO_6 i.e. ν [(M–O–Li)], the weak band around 430 cm^{-1} is assigned for the asymmetric stretching of Li–O in LiO_6 environments. The structure of the synthesized sample by the ion-exchange reaction was further characterized by FT-IR. Figure 4(b) shows the IR spectra of the synthesized sample prepared by solid state reaction method at air atmosphere. It can be seen that strong absorption peaks are observed in the region 400-1000 cm^{-1}. The typical absorption peaks at 515.2 cm^{-1} and 859.4 cm^{-1} which are in agreement with those for $LiNi_{0.8}Co_{0.1}Mn_{0.1}O_2$ prepared by solid-state reaction at high temperature, are observed. The $LiNi_{0.8}Co_{0.1}Mn_{0.1}O_2$ crystal can be considered to be composite metallic oxidant in which Li-ion layer is sandwiched between Ni, Co and Mn and O layers.

Optical properties

It was carried out by measuring the diffuse reflectance spectroscopy in UV-Vis range. The spectrum was taken in the range of 200-700 nm. Fig.1 shows the prepared $LiN_{0.8}Co_{0.1}Mn_{0.1}O_2$ nano-powders synthesized by sol-gel auto-combustion method of the diffused reflectance spectra (absorbance as a function of wavelength). The absorption edges are homogeneous with no other band observed, which confirm that the prepared samples (both methods) are $LiN_{0.8}Co_{0.1}Mn_{0.1}O_2$ layered structure. Those absorption band at around 364.5 nm to 385.5 nm may be due to the MO (M=Ni, Co and Mn) nanoparticles. The absorption edge of the bulk spinel cathode material is around 320 nm and 472 nm [31-32]. The band gap energy was calculated from the diffuse-reflectance spectra by plotting the square of the Kubelka-Munk function given as [33],

$$\boldsymbol{K = \frac{(1-R)^2}{2R}}$$

where *K* is reflectance transformed according to Kubelka Munk, R is reflectancy (%), ***hv*** is the photon energy. The E_g were measured with the help of reflectance spectra plotting graphs of $(K^{*}\boldsymbol{hv})^n$ versus (***hv***).

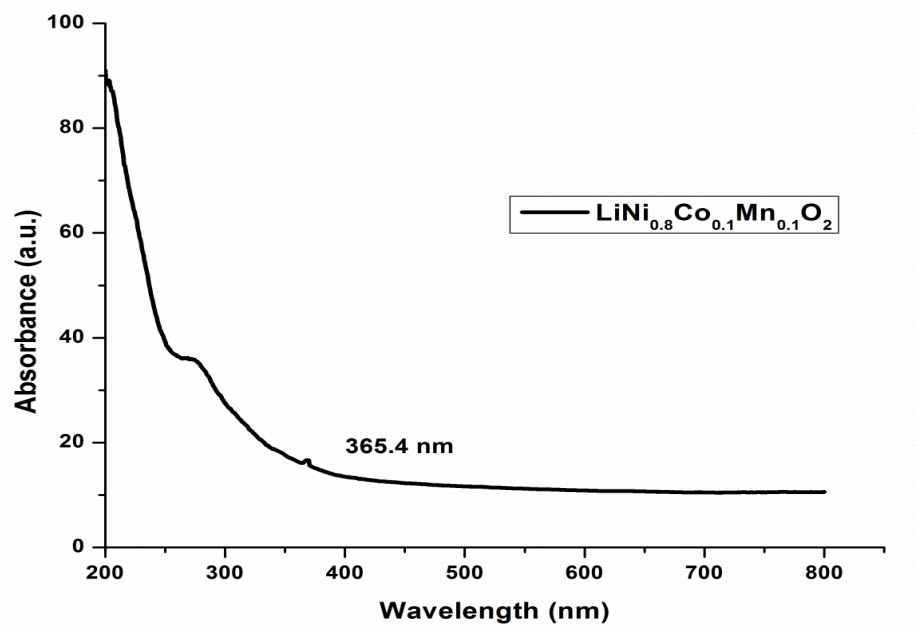

Figure 1:-UV-visible spectra of $LiNi_{0.8}Co_{0.1}Mn_{0.1}O_2$ material is prepared by sol-gel auto-combustion

Conclusions:-

The layered structure material $LiNi_{0.8}Co_{0.1}Mn_{0.1}O_2$ is synthesized by sol-gel auto-combustion and solid-state reaction method. The cathode material resembled the hexagonal α-$NaFeO_2$ structure which was confirmed from the XRD pattern. This result strongly supports the results obtained for the preparation method is sol-gel.

References:-

1. J. Eom, M.G. Kim, J. ChoStorage characteristics of $LiNi_{0.8}Co_{0.1+x}Mn_{0.1-x}O_2$ (x=0, 0.03, and 0.06) cathode materials for Lithium batteries, J. Electrochem. Soc., 155 (2008), p. A239
2. J.-Y. Liao, A. ManthiramSurface-modified concentration-gradient Ni-rich layered oxide cathodes for high-energy lithium-ion batteries, J. Power Sources, 282 (2015), pp. 429-436
3. Y. Su, Y. Yang, L. Chen, Y. Lu, L. Bao, G. Chen, Z. Yang, Q. Zhang, J. Wang, R. Chen, S. Chen, F. WuImprov ing the cycling stability of Ni-rich cathode materials by fabricating surface rock salt phase, Electrochim. Acta, 292 (2018), pp. 217-226
4. J. Fu, D. Mu, B. Wu, J. Bi, H. Cui, H. Yang, H. Wu, F. WuElectrochemical properties of the $LiNi_{0.6}Co_{0.2}Mn_{0.2}O_2$ cathode material modified by Lithium tungstate under high voltage, ACS Appl. Mater. Interfaces, 10 (2018), pp. 19704-19711
5. L. Zhang, H. Wang, L. Wang, Y. CaoHigh electrochemical performance of hollow corn-like $LiNi_{0.8}Co_{0.1}M_{0.1}O_2$ cathode material for lithium-ion batteries, Appl. Surf. Sci., 450 (2018), pp. 461-467

6. S. Chen, T. He, Y. Su, Y. Lu, L. Bao, L. Chen, Q. Zhang, J. Wang, R. Chen, F. WuNi-rich $LiNi_{0.8}Co_{0.1}Mn_{0.1}O_2$ oxide coated by dual-conductive layers as high performance cathode material for Lithium-ion batteries, ACS Appl. Mater. Interfaces, 9 (2017), pp. 29732-29743
7. X. Xiong, Z. Wang, P. Yue, H. Guo, F. Wu, J. Wang, X. LiWashing effects on electrochemical performance and storage characteristics of $LiNi_{0.8}Co_{0.1}Mn_{0.1}O_2$ as cathode material for lithium-ion batteries, J. Power Sources, 222 (2013), pp. 318-325
8. T. Li, X. Li, Z. Wang, H. GuoA short process for the efficient utilization of transition-metal chlorides in lithium-ion batteries: a case of $Ni_{0.8}Co_{0.1}Mn_{0.1}O_{1.1}$ and $LiNi_{0.8}Co_{0.1}Mn_{0.1}O_2$, J. Power Sources, 342 (2017), pp. 495-503
9. Y. Su, G. Chen, L. Chen, W. Li, Q. Zhang, Z. Yang, Y. Lu, L. Bao, J. Tan, R. ChenExposing the {010} planes by oriented self-assembly with nanosheets to improve the electrochemical performances of Ni-Rich $Li[Ni_{0.8}Co_{0.1}Mn_{0.1}]O_2$ microspheres, ACS Appl. Mater. Interfaces, 10 (2018), pp. 6307-6414.
10. Du R., Bi Y., Yang W., Peng Z., Liu M., Liu Y., Wu B., Yang B., Ding F., Wang D.Improved cyclic stability of $LiNi_{0.8}Co_{0.1}Mn_{0.1}O_2$ via Ti substitution with a cut-off potential of 4.5V, Ceram Int, 41 (2015), pp. 7133-7139
11. J. Cho, T.-J. Kim, J. Kim, M. Noh, B. ParkSynthesis, thermal, and electrochemical properties of AlPO4-coated LiNi0.8Co0.1Mn0.1 O 2 cathode materials for a Li-Ion Cell, J. Electrochem. Soc., 151 (2004) A1899-A1904
12. Y. Huang, X. Zhang, R. Yu, S. Jamil, S. Cao, S. Fang, Y. Wang, K. Tang, G. Chen, Z. Luo, X. Yang, X. WangP reparation and performance of the heterostructured material with a Ni-rich layered oxide core and a LiNi0.5Mn1.5O4-like spinel shell, ACS Appl. Mater. Interfaces, 11 (2019), pp. 16556-16566
13. H. Kim, M.G. Kim, H.Y. Jeong, H. Nam, J. ChoA new coating method for alleviating surface degradation of LiNi0.6Co0.2Mn0.2O2 cathode material: nanoscale surface treatment of primary particles, Nano Lett., 15 (2015), pp. 2111-2119
14. J.Y. Liao, A. ManthiramSurface-modified concentration-gradient Ni-rich layered oxide cathodes for high-energy lithium-ion batteries, J. Power Sources, 282 (2015), pp. 429-436
15. Z. Chen, G.-T. Kim, Y. Guang, D. Bresser, T. Diemant, Y. Huang, M. Copley, R.J. Behm, S. Passerini, Z. ShenManganese phosphate coated Li[Ni0.6Co0.2Mn0.2]O2 cathode material: towards superior cycling stability at elevated temperature and high voltage, J. Power Sources, 402 (2018), pp. 263-271
16. X. Xiong, Z. Wang, H. Guo, Q. Zhang, X. LiEnhanced electrochemical properties of lithium-reactive V_2O_5 coated on the $LiNi_{0.8}Co_{0.1}Mn_{0.1}O_2$ cathode material for lithium ion batteries at 60 °C, J. Mater. Chem. A, 1 (2012), pp. 1284-1288.
17. J. Cho, H. Kim, B. ParkComparison of overcharge behavior of $AlPO_4$ -coated $LiCoO_2$ and $LiNi_{0.8}Co_{0.1}Mn_{0.1}O_2$ cathode Materials in Li-Ion Cells, J. Electrochem. Soc., 151 (2004).
18. S.W. Lee, M.S. Kim, J.H. Jeong, D.H. Kim, K.Y. Chung, K.C. Roh, K.B. KimLi_3PO_4 surface coating on Ni-rich $LiNi_{0.6}Co_{0.2}Mn_{0.2}O_2$ by a citric acid assisted sol-gel method: improved thermal stability and high-voltage performance, J. Power Sources, 360 (2017), pp. 206-214.
19. J.D. Steiner, L. Mu, J. Walsh, M.M. Rahman, B. Zydlewski, F.M. Michel, H.L. Xin, D. Nordlund, F. LinAccele rated evolution of surface chemistry determined by temperature and cycling history in nickel-rich layered cathode materials, ACS Appl. Mater. Interfaces, 10 (2018), pp. 23842-23850
20. P. Yan, J. Zheng, J. Liu, B. Wang, X. Cheng, Y. Zhang, X. Sun, C. Wang, J.-G. ZhangTailoring grain boundary structures and chemistry of Ni-rich layered cathodes for enhanced cycle stability of lithium-ion batteries, Nature Energy, 3 (2018), pp. 600-605.
21. L.S. Zhang, K. Jin, L.Z. Wang, Y. Zhang, X.F. Li, Y.H. Song High capacity $Li_{1.2}Mn_{0.54}Ni_{0.13}Co_{0.13}O_2$ cathode materials synthesized using mesocrystal precursors for lithium-ion batteries, J. Alloys Compd., 638 (2015), pp. 298-304.
22. L. Zhang, H. Wang, L. Wang, Y. CaoHigh electrochemical performance of hollow corn-like $LiNi_{0.8}Co_{0.1}Mn_{0.1}O_2$ cathode material for lithium-ion batteries, Appl. Surf. Sci., 450 (2018), pp. 461-467
23. Min Nie, Yunfei Xia, Zhenbo Wang, Fuda Yu, Yin Zhang, Jin Wu, Bing WuEffects of precursor particle size on the performance of $LiNi_{0.5}Co_{0.2}Mn_{0.3}O_2$ cathode material, Ceram. Int., 41 (2015), pp. 15185-15192
24. Ilkyu Hwang, Chul Wee Lee, Jae Chang Kim, Songhun YoonParticle size effect of Ni-rich cathode materials on lithium ion battery performance Mater. Res. Bull., 47 (2012), pp. 73-78
25. Minmin Chen, Enyue Zhao, Dongfeng Chen, Meimei Wu, Songbai Han, Qingzhen Huang, Limei Yang, Xiaolin g Xiao, Zhongbo HuDecreasing Li/Ni disorder and improving the electrochemical performances of Ni-rich $LiNi_{0.8}Co_{0.1}Mn_{0.1}O_2$ by Ca doping, Inorg. Chem., 56 (2017), pp. 8355-8362
26. Duc-luong Vu, Jae-won LeeNa-doped layered $LiNi_{0.8}Co_{0.1}Mn_{0.1}O_2$ with improved rate capability and cycling stability, J. Solid State Electrochem., 22 (2018), pp. 1165-1173

27. Kang Wu, Guofeng Jia, Xuehui Shangguan, Guowei Yang, Zenghu Zhu, Zhengjun Peng, Qin Zhuge, Faqiang L i, Xiaoling CuiImproved high rate performance and cycle stability for $LiNi_{0.8}Co_{0.2}O_2$ by doping of the high valence state ion Nb^{5+} into Li^+ sites, J. Alloy. Comp., 765 (2018), pp. 700-709
28. H.Q. Pham, G. Kim, H.M. Jung, S.-W. Song, Adv. Funct. Mater., 28 (2018), p. 1704690
29. G. Socrates, Infrared Characteristic Group Frequencies, Table and Charts, (second ed.), John Wiley& Sons, New York (1994)
30. A. Vijayamari, K. Sadayandi, Suresh Sagadevan, Preeti Singh, J. Mater. Sci.: Mater. Electron., 28 (2017), pp. 2739-2746.
31. Lehlohonolo F. Koao, Setumo V. Motloung, Tshwafo E. Motaung, Mesfin A. Kebede, Physica B: Condensed Matter, 535 (2018) 323-329.
32. H. Bai, Z. Liu, D.D. Sun, Int. J. Hydrog. Energy, 37 (2012), pp. 13998-14008.